THE JOURNAL OF BIOLOGICAL CHEMISTRY VOL. 289, NO. 36, pp. 24944–24955, September 5, 2014

Proteasome Dysfunction Activates Autophagy and the Keap1-Nrf2 Pathway*

Received for publication, May 10, 2014, and in revised form, July 14, 2014 Published, JBC Papers in Press, July 21, 2014, DOI 10.1074/jbc.M114.580357

Shun Kageyama[‡§], Yu-shin Sou[§], Takefumi Uemura[¶], Satoshi Kametaka[¶], Tetsuya Saito[‡‖], Ryosuke Ishimura[‡‖], Tsuguka Kouno[§], Lynn Bedford[**], R. John Mayer[**], Myung-Shik Lee[‡‡], Masayuki Yamamoto[§§], Satoshi Waguri[¶], Keiji Tanaka[‖], and Masaaki Komatsu[‡§1]

From the [‡]Department of Biochemistry, School of Medicine, Niigata University, Chuo-ku, Niigata 951-8510, Japan, the [§]Protein Metabolism Project and [‖]Laboratory of Protein Metabolism, Tokyo Metropolitan Institute of Medical Science, Setagaya-ku, Tokyo 156-8506, Japan, the [¶]Department of Anatomy and Histology, Fukushima Medical University School of Medicine, Hikarigaoka, Fukushima 960-1295, Japan, the [**]Laboratory of Intracellular Proteolysis, School of Biomedical Sciences, University of Nottingham, School of Life Sciences, Queen's Medical Centre, Nottingham NG7 2UH, United Kingdom, the [‡‡]Department of Medicine, Samsung Medical Center, Gangnam-gu, Seoul 135-710, Korea, and the [§§]Department of Medical Biochemistry, Tohoku University Graduate School of Medicine, Aoba-ku, Sendai 980-8575, Japan

Background: Malfunctions in the ubiquitin-proteasome system cause accumulation of non-functional, potentially toxic protein aggregates.
Results: The protein aggregates activate Nrf2 and are then excluded by autophagy *in vivo*.
Conclusion: Both Nrf2 and autophagy serve as *in vivo* cellular adaptations to impaired proteasome.
Significance: Cells contain networks of cellular defense mechanisms against defective proteostasis.

The ubiquitin-proteasome system and autophagy are crucially important for proteostasis in cells. These pathways are interdependent, and dysfunction in either pathway causes accumulation of ubiquitin-positive aggregates, a hallmark of human pathological conditions. To elucidate *in vivo* compensatory action(s) against proteasomal dysfunction, we developed mice with reduced proteasome activity in their livers. The mutant mice exhibited severe liver damage, accompanied by formation of aggregates positive for ubiquitin and p62/Sqstm1, an adaptor protein for both selective autophagy and the anti-oxidative Keap1-Nrf2 pathway. These aggregates were selectively entrapped by autophagosomes, and pathological features of livers with impaired proteasome activity were exacerbated by simultaneous suppression of autophagy. In contrast, concomitant loss of *p62*/*Sqstm1* had no apparent effect on the liver pathology though p62/Sqstm1 was indispensable for the aggregates formation. Furthermore, defective proteasome function led to transcriptional activation of the Nrf2, which served as a physiological adaptation. Our *in vivo* data suggest that cells contain networks of cellular defense mechanisms against defective proteostasis.

The 26S proteasome, in collaboration with the sophisticated ubiquitination system used for selection of target proteins, is responsible for degrading unnecessary or damaged proteins. Malfunctions in this pathway cause accumulation of non-functional, potentially toxic protein aggregates (1–3). The macroautophagy (hereafter referred to as autophagy) system serves as a supplier of molecular building blocks under starved conditions and also contributes to cellular renovation during cell differentiation (4, 5). Defects in this process can cause amino acid insufficiency, which impairs protein synthesis during adaptation to starvation, as well as energy production essential for cell survival and development (4, 5). Even under nutrient-rich conditions, autophagy occurs constitutively at low levels to mediate global turnover of cytoplasmic materials (6, 7).

Dysfunctions of autophagy coupled to the ubiquitin system have been directly linked to human conditions such as Parkinson disease and inflammatory disorders. Autophagy contributes to selective removal of aggregated proteins (aggrephagy), unnecessary or damaged mitochondria (mitophagy), and invading bacteria (xenophagy); these processes are usually mediated by ubiquitin signaling (8–10). When the ubiquitin-proteasome system is impaired due to accumulation of certain aggregation-prone proteins related to neurodegenerative disease, autophagy is responsible for eliminating ubiquitin-positive protein aggregates (11–13). In response to loss of mitochondrial membrane potential, the E3 ligase Parkin translocates to damaged mitochondria in a PINK1-dependent manner; once it is localized to mitochondria, it ubiquitinates outer membrane proteins, thereby inducing mitophagy (14, 15). Parkinson disease-related mutations of *Parkin* and *PINK1* prevent induction of mitophagy, resulting in persistence of damaged mitochondria, which may play a role in the pathogenesis of Parkinson disease (14, 15). Invading bacteria in the cytosol and/or ruptured endosomal membranes are ubiquitinated by E3s, including Parkin (16) and LRSAM1 (17), which mediates autophagic sequestration of microbes to restrict their growth. Ubiquitin- and LC3-binding adaptor proteins, includ-

* This work was supported by Grant-in-aid for Scientific Research on Innovative Areas 25111006 (to M. K. and S. W.), Funding Program for Next Generation World Leading Researchers Grant LS132 (to M. K.), the Takeda Science Foundation (to T. K. and M. K.), and a Global Research Laboratory grant (to M-S. L. and M. K.).
[1] To whom correspondence should be addressed: Dept. of Biochemistry, School of Medicine, Niigata University, Chuo-ku, Niigata 951-8510, Japan. Tel.: 81-25-277-2077; Fax: 81-25-277-0757, E-mail: komatsu-ms@med.niigata-u.ac.jp.

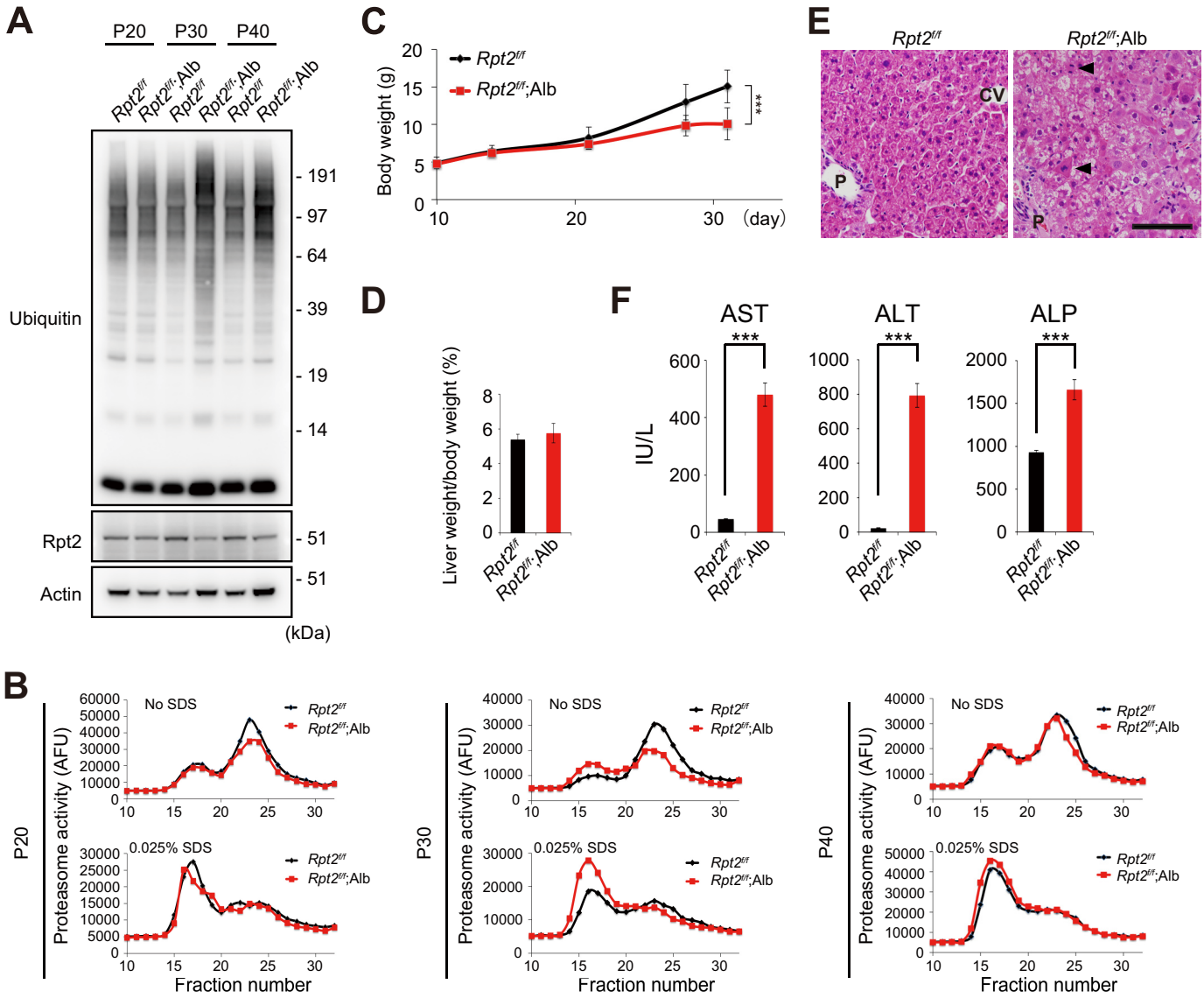

FIGURE 1. **Time course analysis of *Rpt2*$^{f/f}$*;Alb mice.** *A*, liver homogenates were prepared from mice of the indicated genotypes at P20, P30, and P40 and subjected to immunoblotting with the indicated antibodies. Data were obtained from three independent experiments. *B*, proteasome activity in *Rpt2*$^{f/f}$;Alb livers at P20, P30, and P40. *C*, growth curve of *Rpt2*$^{f/f}$ (control) and *Rpt2*$^{f/f}$;Alb mice. Data are means ± S.E. of *Rpt2*$^{f/f}$ ($n = 33$) and *Rpt2*$^{f/f}$;Alb ($n = 24$) mice. ***, $p < 0.001$. *D*, ratio of liver weight to body weight of *Rpt2*$^{f/f}$ (control) and *Rpt2*$^{f/f}$;Alb mice at P30. Data are means ± S.E. of *Rpt2*$^{f/f}$ ($n = 5$) and *Rpt2*$^{f/f}$;Alb ($n = 8$) mice. *E*, H&E staining of livers of indicated genotypes at P30. Mitotic cells or abnormal mitosis (arrowheads) were often observed in *Rpt2*-deficient hepatocytes. *CV*, central vein; *P*, portal triad. *Bar*, 100 μm. *F*, serum levels of aspartate aminotransferase (*AST*), alanine aminotransferase (*ALT*), and alkaline phosphatase (*ALP*) were measured. Data are means ± S.E. of *Rpt2*$^{f/f}$ ($n = 3$) and *Rpt2*$^{f/f}$;Alb ($n = 5$) mice. ***, $p < 0.001$. *IU/L*, international units/liter. *AFU*, arbitrary fluorescent unit.

ing p62/Sqstm1 (hereafter referred to as p62) (18), neighbor of BRCA1 gene 1 (Nbr1)[2] (19), NDP52 (20), and optineurin (21), are translocated to these ubiquitinated cargos; this process is assumed to mediate sequestration of ubiquitinated cargos into autophagosomes. Among them, p62 and Nbr1 have been identified as major components of many types of aggregates or inclusions observed in various human diseases, including neurodegenerative diseases, liver disorders, and hepatocellular carcinomas (19, 22). But significance of such adaptor proteins on the aggregates, particularly *in vivo*, remains unclear.

The Keap1-Nrf2 pathway, one of the major cellular defense mechanisms against oxidative and electrophilic stresses (23, 24), is activated during selective autophagy (25–28). Under normal conditions, the transcription factor Nrf2 (nuclear factor erythroid 2-related factor 2) is constitutively degraded through the ubiquitin-proteasome pathway; its binding partner, Keap1 (kelch-like ECH-associated protein 1), is an adaptor of the ubiquitin ligase complex that targets Nrf2. Exposure to electrophiles, reactive oxygen species, and nitric oxide instigates modification of the cysteine residues of Keap1, leading to its inactivation. As a result, Nrf2 is stabilized, and it subsequently translocates to the nucleus to induce the transcription of numerous cytoprotective genes through heterodimerization with small Maf proteins (23, 24). p62 also regulates the Keap1-

[2] The abbreviations used are: Nbr1, neighbor of BRCA1 gene 1; Keap1, kelch-like ECH-associated protein 1; Nqo1, NAD(P)H dehydrogenase quinone 1; Nrf2, nuclear factor erythroid 2-related factor 2; P, postnatal day.

Nrf2 pathway via a noncanonical mechanism (25–28). Under conditions of selective autophagy, Ser^{403} of the ubiquitin-associated domain of p62 is initially phosphorylated by casein kinase 2 or TANK-binding kinase 1, which promotes the translocation of p62 to cargos positive for ubiquitin (29, 30). Subsequently, Ser^{351} of the Keap1-interacting region of p62 is phos-

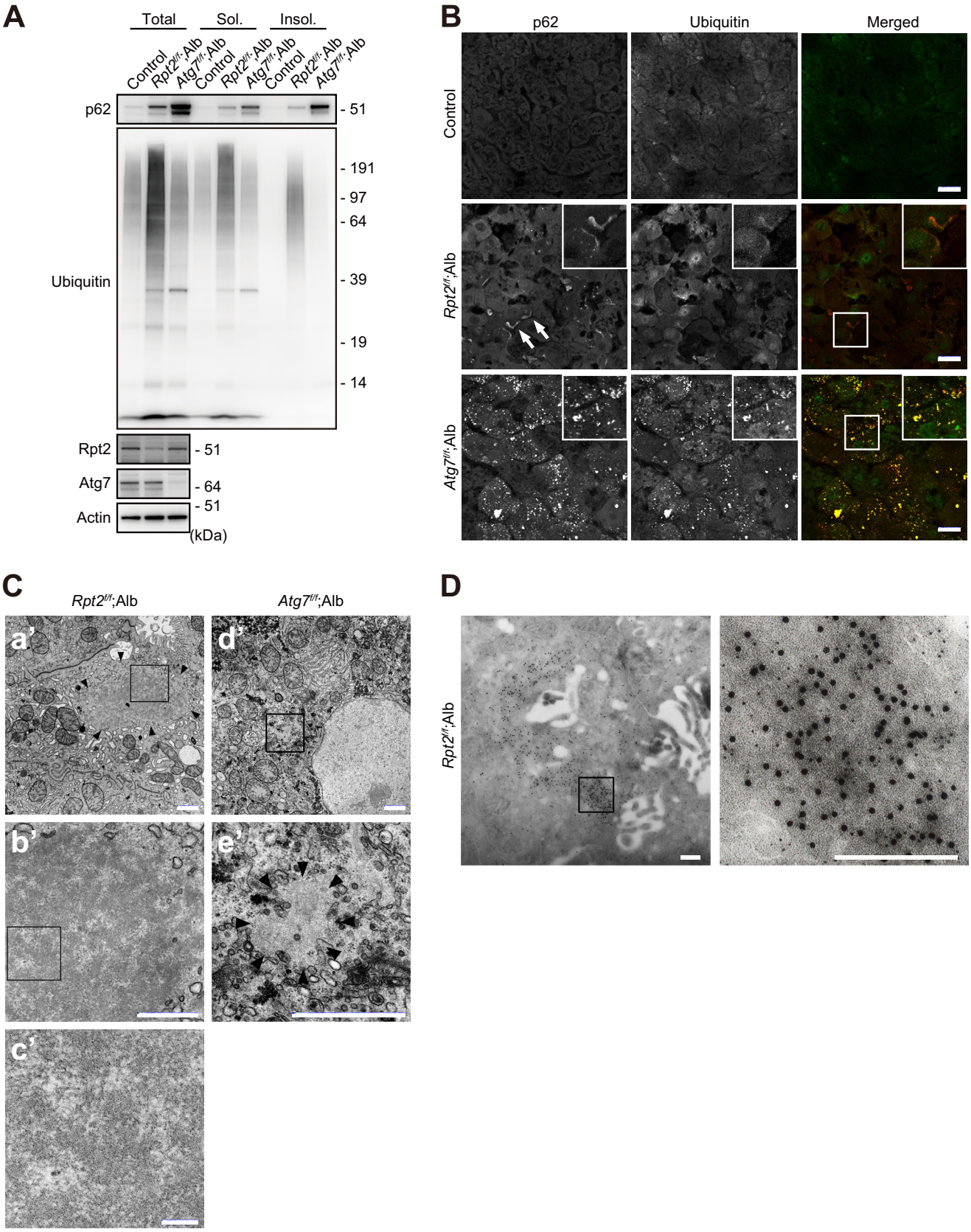

phorylated, followed by sequestration of Keap1 on the cargos. As a result, Nrf2 is stabilized; as in the canonical pathway, it then translocates into the nucleus to induce its cytoprotective target genes (25, 26). The ubiquitinated autophagic cargos, together with phosphorylated p62 and the Keap1 complex, are degraded by autophagy, leading to elimination of cytotoxic components (27). However, the physiological role of the coupling between the Keap1-Nrf2 system and selective autophagy *in vivo* has been not yet determined. In this study, we developed genetically modified mice with decreased 26S proteasome activity, which accumulate aggregate structures positive for both ubiquitin and p62 in their cells, and found that proteasome-dysfunction activates selective autophagy and the Keap1-Nrf2 pathway, both of which serve as cellular defense mechanisms.

EXPERIMENTAL PROCEDURES

Mice—Rpt2$^{flox/flox}$ mice (31) were cross-bred with albumin-*Cre* transgenic mice (32) to generate *Rpt2$^{flox/flox}$*;Alb-*Cre* mice. *Atg7$^{flox/flox}$*, *p62$^{flox/flox}$*, and the *Nrf2*-knock-out mice used in this study were described previously (33–35). Mice were housed in specific pathogen-free facilities, and the Ethics Review Committee for Animal Experimentation of the Tokyo Metropolitan Institute of Medical Science approved the experimental protocols.

Immunoblot Analysis—Immunoblots were carried out as described previously (26). Antibodies against p62 (Progen Biotechnik, GP62-C), ubiquitin (Santa Cruz Biotechnology, Inc., P4D1), Keap1 (Proteintech Group, Inc.), Nqo1 (Abcam, Inc.), Nrf2 (Santa Cruz Biotechnology, Inc., H-300), LC3B (Cell Signaling Technology, catalog no. 2775), Nbr1 (ProteinExpress Co., Ltd.), GFP (Invitrogen), actin (Chemicon Intl., Inc., MAB1501R), and lamin B (Santa Cruz Biotechnology, Inc., M-20) were purchased from the indicated suppliers. Anti-phosphorylated p62 polyclonal antibody was raised in rabbits using the peptide Cys+KEVDP(pS)TGELQSL as an antigen (26). The rabbit polyclonal antibodies against Atg7 and Rpt2 were described previously (36, 37).

Assay of Proteasome Activity—Peptidase activity was measured using a fluorescent peptide substrate, succinyl-Leu-Leu-Val-Tyr-7-amido-4-methylcoumarin (Suc-LLVY-MCA), as described previously (38).

Histological Examination—Fixation and embedding procedures for immunohistochemistry were described previously (39). Briefly, mouse livers were quickly excised, cut into small pieces, and then fixed by immersion in 4% paraformaldehyde/4% sucrose in 0.1 M phosphate buffer, pH 7.4 (PB). After rinsing, samples were embedded in paraffin (for H&E staining), or in OCT compound (for immunofluorescence). For immunofluorescence microscopy, sections were blocked and then incubated for 2–3 days at 4 °C with the following primary antibodies: guinea pig polyclonal antibody against p62 (Progen), rabbit polyclonal antibody against ubiquitin (DAKO), or rabbit polyclonal antibody against Keap1 (Proteintech Group). Immunofluorescence images were taken with an FV1000 laser scanning confocal microscope equipped with a UPlanSApo 40× numerical aperture 1.3 oil objective lens (Olympus). After image acquisition, contrast and brightness were adjusted using Photoshop CS4.

Electron Microscopy and Immunoelectron Microscopy—For conventional electron microscopy, livers were excised and fixed by immersion in 0.1 M PB containing 2% paraformaldehyde and 2% glutaraldehyde. Fixed samples were post-fixed with 1% OsO_4, embedded in Epon812, and sectioned. Immunoelectron microscopy was carried out on ultrathin cryosections, as described previously (39). In brief, livers were fixed by cardiac perfusion with 0.1 M PB containing 4% paraformaldehyde and 4% sucrose and then frozen in PB with 2.3 M sucrose and 20% polyvinylpyrrolidone. Ultrathin sections were mounted on Formvar carbon-coated nickel grids, blocked with 1% bovine serum albumin in PBS, incubated with anti-ubiquitin (DAKO) and anti-p62 (Progen) antibodies, and then incubated with colloidal gold-conjugated secondary antibodies.

Quantitative Real-time PCR—Using the Transcriptor First-Strand cDNA Synthesis Kit (Roche Applied Science), cDNA was synthesized from 1 μg of total RNA. Quantitative PCR was performed using LightCycler® 480 Probes Master mix (Roche Applied Science) on a LightCycler® 480 (Roche Applied Science). Signals were normalized against that of β-glucuronidase (*Gus*). The sequences of the primers used were as follows: *Nqo1* (left), AGCGTTCGGTATTACGATCC; *Nqo1* (right), AGTACAATCAGGGCTCTTCTCG.

Statistical analysis—Values, including those displayed in the graphs, are means ± S.E. Statistical analysis was performed using the unpaired *t* test (Welch test). *p* values less than 0.05 denoted statistical significance.

RESULTS

Generation of Mice with Decreased Proteasome Activity—To investigate aggrephagy *in vivo*, we crossbred mice bearing a conditional knock-out of *Rpt2*, one of six ATPases of the 19S regulatory particle of the 26S proteasome (*Rpt2$^{flox/flox}$*) (31), with albumin-*Cre* (Alb-*Cre*) transgenic mice (32). The *Rpt2$^{flox/flox}$*;Alb-*Cre* (*Rpt2$^{f/f}$*;Alb) mice were viable at birth and indistinguishable in appearance from their littermates. In *Rpt2$^{f/f}$*;Alb mice, levels of Rpt2 protein in the liver started to decrease at postnatal day (P)30 and recovered at P40 (Fig. 1*A*); ubiquitinated proteins accumulated significantly in the liver at P30 (Fig. 1*A*). The chymotryptic activities of the 26S and 20S proteasomes (measured using Suc-LLVY-MCA as a substrate)

FIGURE 2. **Characterization of ubiquitinated aggregates in *Rpt2$^{f/f}$;Alb* livers.** *A*, liver homogenates were prepared from mice of the indicated genotypes at P30. Total, soluble (*Sol.*), and insoluble (*Insol.*) fractions were subjected to immunoblotting with the indicated antibodies. Data were obtained from three independent experiments. *B*, liver cryosections from mice of the indicated genotypes at P30 were double-immunostained with p62 and ubiquitin antibodies. A portion of each image is magnified and shown in the *inset*. *Arrows* indicate large pleomorphic aggregated structures. Merged images are shown at the *right column* (*red*, p62; *green*, ubiquitin). *Bars*, 20 μm. *C*, electron micrographs of hepatocytes of the indicated genotypes. The *boxed* regions in *a′*, *b′*, and *d′* are enlarged and shown in *b′*, *c′*, and *e′*, respectively. *Arrowheads* indicate aggregated structures. *Bars*, *a′*, 1 μm; *b′* and *c′*, 0.5 μm; *d′*, 0.1 μm. *D*, immunoelectron micrographs showing double labeling of ubiquitin (12-nm colloidal gold particles) and p62 (6-nm colloidal gold particles) in hepatocytes of *Rpt2$^{f/f}$*;Alb mice at P30. The *boxed* region is *enlarged* and shown at the *right*. *Bars*, 0.2 μm.

in extracts from *Rpt2*$^{f/f}$;Alb livers at P20 were comparable with those in age-matched control livers (Fig. 1*B*). The activity of the 26S proteasome decreased dramatically at P30 and recovered at P40, whereas the activity of the 20S proteasome increased at P30 only (Fig. 1*B*). Consistent with these kinetics, growth retardation was observed as early as at P30 (Fig. 1*C*). Although the

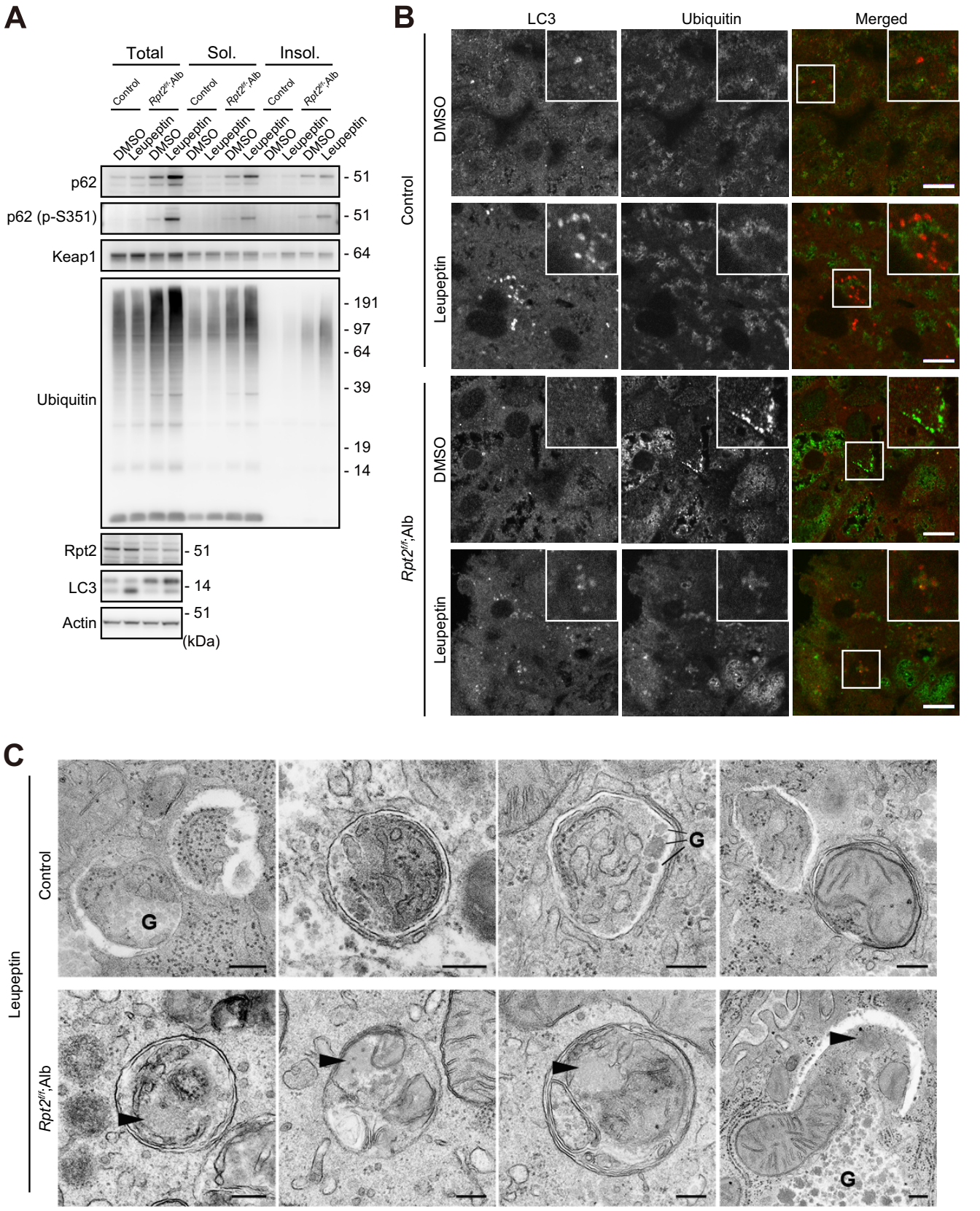

ratio of liver weight to body weight was similar among genotypes even at P30 (Fig. 1*D*), decreased proteasome activity in *Rpt2*$^{f/f}$;Alb livers was accompanied by signs of hepatic degeneration such as the presence of hypertrophic cells, dead cells, small regenerating cells, and inflammatory cells, as revealed by hematoxylin and eosin (H&E) staining (Fig. 1*E*) and by hepatocytic damage, as revealed by leakage of liver enzymes (Fig. 1*F*). The recovery of *Rpt2* at P40 in the livers of *Rpt2*$^{f/f}$;Alb mice might be attributed to rapid hepatocytic death due to impairment of proteasome activity, followed by compensatory regeneration of hepatocytes from oval cells, which express low levels of albumin (40). Collectively, these data indicate that at P30, *Rpt2*$^{f/f}$;Alb mice exhibit liver injury accompanied by reduced proteasome activity in the liver.

Characterization of Ubiquitinated Aggregates in Rpt2$^{f/f}$*;Alb Livers*—Immunoblot analysis revealed elevated levels of both soluble and insoluble ubiquitinated proteins in the livers of *Rpt2*$^{f/f}$;Alb mice (Fig. 2*A*). The level of insoluble ubiquitinated proteins was significantly higher in *Rpt2*$^{f/f}$;Alb than in *Atg7*$^{flox/flox}$;Alb-*Cre* (*Atg7*$^{f/f}$;Alb) livers, in which autophagy is impaired (Fig. 2*A*) (33). We also observed significant accumulation of p62 protein in both detergent-soluble and -insoluble fractions from *Rpt2*$^{f/f}$;Alb livers, albeit less than in *Atg7*$^{f/f}$;Alb liver fractions (Fig. 2*A*). Consistent with these biochemical data, immunofluorescence analysis revealed co-localization of ubiquitin and p62 on large pleomorphic aggregated structures and small punctate structures in *Rpt2*$^{f/f}$;Alb hepatocytes (Fig. 2*B*). As in a previous study (33), aggregates observed in *Atg7*$^{f/f}$;Alb hepatocytes were also positive for ubiquitin and p62 (Fig. 2*B*). Electron microscopy revealed that *Rpt2*$^{f/f}$;Alb hepatocytes contained large pleomorphic structures mainly consisting of electron-lucent areas and scattered patchy electron-dense areas; this pattern appeared to be formed by the clustering of fibrillar elements (Fig. 2*C*). These features were distinct from the large circular or elliptical structures often observed in *Atg7*$^{f/f}$;Alb hepatocytes (Fig. 2*C*). By double-immunoelectron microscopy, we confirmed the co-localization of p62 and ubiquitin in the cytoplasmic aggregated structures in *Rpt2*$^{f/f}$;Alb hepatocytes (Fig. 2*D*). Colloidal gold particles representing ubiquitin were distributed in highly electron-dense areas, whereas particles representing p62 were distributed in areas of both high and low electron density.

Induction of Aggrephagy in Rpt2$^{f/f}$*;Alb Livers*—We next examined autophagic flux in livers of *Rpt2*$^{f/f}$;Alb mice. Intraperitoneal (i.p.) injection of leupeptin, a lysosomal cysteine proteinase inhibitor, resulted in elevation of LC3-II (an indicator of autophagic flux) (41) in livers of both control and *Rpt2*$^{f/f}$;Alb mice, although the effect was smaller in the mutants (Fig. 3*A*). The levels of ubiquitinated proteins and p62 in mutant livers further increased upon intraperitoneal injection of leupeptin, but this effect was not observed in control livers (Fig. 3*A*). Phosphorylation of p62 at Ser^{351}, which signifies induction of selective autophagy (26), increased only in the intraperitoneally injected mutant livers (Fig. 3*A*), implying increased selective autophagy of aggregate structures (aggrephagy). Indeed, immunofluorescence analysis revealed that LC3/ubiquitin double-positive structures were frequently observed in leupeptin-treated *Rpt2*$^{f/f}$;Alb mice (8.23%), whereas they could barely be detected in leupeptin-treated control hepatocytes (2.68%) (Fig. 3*B*). Furthermore, we confirmed by electron microscopy that autophagosomes in the mutant hepatocytes occasionally (*arrowheads*; 7/46, 15.2%) contained aggregate-like amorphous structures, whereas those in control hepatocytes did not (0/64; 0%) (Fig. 3*C*).

Exacerbation of Liver Pathology in Rpt2$^{f/f}$*;Alb Mice by Suppression of Autophagy*—Next, to clarify the physiological significance of autophagy induced in *Rpt2*$^{f/f}$;Alb liver, we generated hepatocyte-specific *Rpt2* and *Atg7* double-knock-out mice (*Rpt2*$^{f/f}$;*Atg7*$^{f/f}$;Alb). Concomitant loss of *Atg7* in *Rpt2*$^{f/f}$;Alb mice resulted in dramatic accumulation of soluble and insoluble p62 (Fig. 4*A*), supporting the evidence p62 is a selective substrate for autophagy (18, 33) and gene expression of *p62* is induced by impairment of autophagy (25). Meanwhile, ubiquitinated proteins were present in detergent-soluble and -insoluble fractions of *Rpt2*$^{f/f}$;*Atg7*$^{f/f}$;Alb livers to a similar extent in those of *Rpt2*$^{f/f}$;Alb livers (Fig. 4*A*). This observation might be attributed to more severe hepatic damage in the double-mutant livers (see below). In the absence of *Atg7*, the large pleomorphic aggregates positive for ubiquitin and p62 observed in *Rpt2*$^{f/f}$;Alb hepatocytes became small, round, and scattered throughout the cytoplasm (Fig. 4, *B* and *C*), similar to structures observed in autophagy-deficient livers (Figs. 2*B* and 4*B*). In addition, liver damage due to impaired proteasome activity was more severe than in *Atg7*$^{f/f}$;Alb mice, and the damage was exacerbated by simultaneous loss of *Atg7*. The growth delay in *Rpt2*$^{f/f}$;*Atg7*$^{f/f}$;Alb mice was more severe than in *Rpt2*$^{f/f}$;Alb or *Atg7*$^{f/f}$;Alb mice (Fig. 4*D*). Furthermore, we observed hepatomegaly accompanied by cellular hypertrophy and degeneration, both typical phenotypes of autophagy-deficient livers (33), in hepatocytes of *Rpt2*$^{f/f}$;*Atg7*$^{f/f}$;Alb mice (Fig. 4, *E* and *F*). The *Rpt2*$^{f/f}$;*Atg7*$^{f/f}$;Alb mice exhibited higher serum levels of aspartate aminotransferase, alanine aminotransferase, and alkaline phosphatase than single *Atg7*- or *Rpt2*-knock-out mice (Fig. 4*G*).

Feedback Activation of the Keap1-Nrf2 Pathway when the Proteasome Is Impaired—We postulated that under proteasome-defective conditions, the Keap1-Nrf2 pathway should be activated in a p62 phosphorylation-dependent manner. In fact, we observed accumulation of not only p62, but also its Ser^{351}-phosphorylated form, in *Rpt2*$^{f/f}$;Alb livers (Figs. 2*A* and 5*A*). A significant proportion of Ser^{351}-phosphorylated p62 was recovered in the detergent-insoluble fraction (Figs. 2*A* and 5*A*), and

FIGURE 3. **Autophagic degradation of ubiquitin-positive aggregates accumulated due to impaired proteasome activity.** *A*, mice of the indicated genotypes were subjected to intraperitoneal injection of leupeptin at P30. One hour after the injection, liver homogenates were prepared and subjected to immunoblotting with the indicated antibodies. Data were obtained from three independent experiments. A graph indicates quantitative densitometry of immunoblotting data ($n = 3$) and the ratios of insoluble (*Insol.*) ubiquitinated proteins relative to that of dimethyl sulfoxide (*DMSO*)-treated control mice. *B*, liver cryosections from mice of the indicated genotypes treated as described in *A* were double-immunostained with LC3 (*red* in the merged image) and ubiquitin (*green* in the merged image) antibodies. The *boxed* region is magnified and shown in the *inset*. *Bars*, 10 μm. *C*, electron micrographs of hepatocytes from mice of the indicated genotypes, treated as described in *A*. *Arrowheads*, aggregate-like amorphous structures. *G*, glycogen granules. *Bar*, 0.2 μm. *Sol.*, soluble.

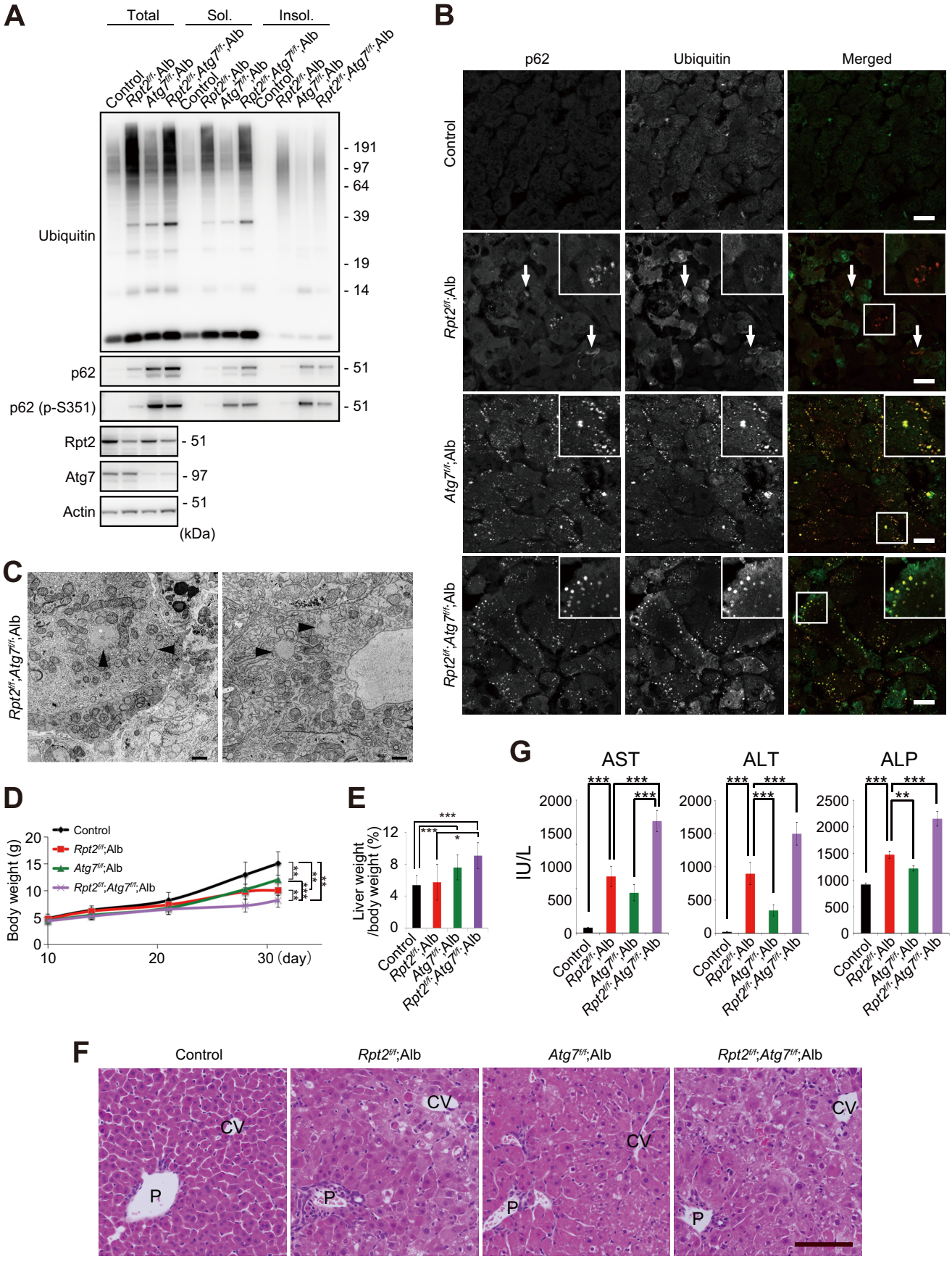
A
Total
Sol.
Insol.
Control
Rpt2f/f;Alb
Atg7f/f;Alb
Rpt2f/f;Atg7f/f;Alb
Ubiquitin
p62
p62 (p-S351)
Rpt2
Atg7
Actin
- 191
- 97
- 64
- 39
- 19
- 14
- 51
- 51
- 51
- 97
- 51
(kDa)
B
p62
Ubiquitin
Merged
Control
Rpt2f/f;Alb
Atg7f/f;Alb
Rpt2f/f;Atg7f/f;Alb
C
Rpt2f/f;Atg7f/f;Alb
D
Control
Rpt2f/f;Alb
Atg7f/f;Alb
Rpt2f/f;Atg7f/f;Alb
Body weight (g)
20
15
10
5
0
10
20
30 (day)
E
Liver weight /body weight (%)
12
8
4
0
Control
Rpt2f/f;Alb
Atg7f/f;Alb
Rpt2f/f;Atg7f/f;Alb
G
AST
ALT
ALP
IU/L
2000
1500
1000
500
0
2500
F
Control
Rpt2f/f;Alb
Atg7f/f;Alb
Rpt2f/f;Atg7f/f;Alb
CV
P

Keap1 was also recovered in the detergent-insoluble fraction (Fig. 5*A*). At the same time, Nrf2 was stabilized in the mutant livers (Fig. 5*A*). Immunofluorescence analysis revealed extensive co-localization of p62 and Keap1 in the same aggregate structures (Fig. 5*B*). Consequently, gene expression of the Nrf2 target gene *Nqo1* (NAD(P)H dehydrogenase quinone 1) in the livers of *Rpt2*$^{f/f}$;Alb mice was markedly induced (Fig. 5*C*), and we also observed increased levels of Nqo1 protein (Fig. 5*A*). As expected, loss of *Nrf2* in *Rpt2*$^{f/f}$;Alb mice suppressed induction of Nrf2 targets (Fig. 5, *A* and *C*). p62 was present at higher levels in *Rpt2*$^{flox/flox}$;*Nrf2*$^{-/-}$;Alb-*Cre* (*Rpt2*$^{f/f}$;*Nrf2*$^{-/-}$;Alb) than in control livers (Fig. 5*A*). Therefore, as in *Rpt2*$^{f/f}$;Alb livers, aggregate structures positive for both p62 and Keap1 were detected in hepatocytes of *Rpt2*$^{f/f}$;*Nrf2*$^{-/-}$;Alb mice (Fig. 5*B*). The double mutant mice exhibited slower growth than *Rpt2*$^{f/f}$;Alb mice, whereas single knock-out of *Nrf2* hardly affected growth, at least at P30 (Fig. 5*D*). H&E staining revealed no significant difference between control and *Nrf2* single knock-out livers; by contrast, simultaneous loss of *Nrf2* and *Rpt2* in the liver caused degenerative alterations more severe than those observed in *Rpt2* single knock-out livers (Fig. 5*E*), and leakage of hepatic enzymes into sera was more severe in double knock-out (*Rpt2*$^{f/f}$;*Nrf2*$^{-/-}$;Alb) mice than in *Rpt2*$^{f/f}$;Alb mice (Fig. 5*F*).

Role of p62 in Formation of Aggregate-containing Structures in Rpt2$^{f/f}$*;Alb Hepatocytes*—To investigate the effect of loss of *p62* on aggregate formation, Nrf2 activation and pathology in mice with decreased proteasome activity, we generated hepatocyte-specific *Rpt2* and *p62* double-knock-out mice (*Rpt2*$^{f/f}$;*p62*$^{f/f}$;Alb). The levels of total ubiquitinated proteins in livers of *Rpt2*$^{f/f}$;*p62*$^{f/f}$;Alb mice were similar to those in *Rpt2*$^{f/f}$;Alb livers (Fig. 6*A*). The accumulation of insoluble ubiquitinated proteins in *Rpt2*$^{f/f}$;Alb mice was dramatically suppressed by loss of *p62* (Fig. 6*A*). Although the number of aggregates was reduced by deletion of *p62*, we still occasionally detected large pleomorphic aggregates positive for ubiquitin, even in *Rpt2*$^{f/f}$;*p62*$^{f/f}$;Alb hepatocytes, by immunofluorescence staining (Fig. 6*B*). In electron micrographs, the aggregated structures appeared rather homogeneous, containing less electron-dense areas than those in *Rpt2*$^{f/f}$;Alb hepatocytes (Fig. 6*C*). We speculated that Nrf2-activation observed in single *Rpt2*-deficient livers was abrogated by concomitant loss of *p62*. The nuclear translocation as well as induction of Nqo1 tended to be inhibited by simultaneous loss of *p62*, but we did not recognize any significant differences (Fig. 6, *A* and *D*). *Rpt2*$^{f/f}$;*p62*$^{f/f}$;Alb pups were born at Mendelian frequency, and their growth was delayed similarly to that of *Rpt2*$^{f/f}$;Alb mice (Fig. 7*A*). Histological analysis revealed degenerated features in *Rpt2*$^{f/f}$;*p62*$^{f/f}$;Alb livers similar to those observed in *Rpt2*-deficient livers, although hepatocytic hypertrophy tended to be ameliorated (Fig. 7*B*). Leakage of hepatic enzymes in *Rpt2*$^{f/f}$;*p62*$^{f/f}$;Alb was detected at a level similar to that in single *Rpt2* knock-out mice (Fig. 7*C*).

DISCUSSION

In this study, we showed that reduced proteasome activity caused formation of aggregate structures positive for ubiquitin and p62 (Fig. 2) and then activated not only aggrephagy but also the Keap1-Nrf2 pathway (Figs. 3 and 5). Simultaneous suppression of autophagy in proteasome-suppressed livers induced accumulation of p62; in addition, the large pleomorphic p62- and ubiquitin-positive aggregates found in proteasome-suppressed livers became small and round (Fig. 4, *B* and *C*). Meanwhile, additional loss of *p62* in hepatocytes with impaired proteasome activity greatly reduced the level of ubiquitin-positive aggregates with altered morphological compositions (Fig. 6, *A*–*C*). Because the fibril-like structures were recognized even in *Rpt2*/*p62* double-deficient hepatocytes (Fig. 6*C*), we concluded that cellular levels of p62 determine the morphological characteristics of ubiquitin aggregates but not the primarily formation of fibril-like structures.

What is the physiological significance of p62 on these aggregates? One possibility is that p62 serves a receptor function in aggrephagy; this idea is supported by the observation that ubiquitin aggregates positive for p62 were degraded in an autophagy-dependent manner (Fig. 3). However, additional loss of *Atg7*, but not *p62*, exacerbated the pathology in proteasome-defective liver (Figs. 4 and 7), suggesting that p62 is not involved in recognition of the aggregates. Although there remains a possibility that Nbr1, whose domain structure is quite similar to that of p62 (8), compensates the function of p62, simultaneous loss of *Nbr1* in *p62*-deficient livers did not exhibit any accumulation of ubiquitinated proteins in contrast to defective autophagy.[3] Another possibility is that p62 serves as a scaffold for Nrf2 activation. Ser^{351} of p62 is phosphorylated on cargos destined for autophagy, such as ubiquitin-positive aggregates, and this phosphorylation is followed by robust Nrf2 activation (26). Indeed, we observed p62 phosphorylation and subsequent Nrf2 activation in livers with decreased proteasome activity (Fig. 5, *A* and *C*). However, additional loss of *Nrf2* (Fig. 5), but not of *p62* (Fig. 7), exacerbated the pathological state caused by inhibition of proteasome activity. This discrepancy can be explained by the fact that Nrf2 degradation is dependent on the ubiquitin-proteasome system (23, 24). In *Rpt2*/*p62* double knock-out livers, reduced proteasome activity could directly activate Nrf2 even in the absence of p62 (Fig. 6, *A* and *D*). In

[3] Y.-S. Sou and M. Komatsu, unpublished data.

FIGURE 4. **Exacerbation of pathology in *Rpt2*$^{f/f}$*;Alb* liver by concomitant loss of *Atg7*.** *A*, liver homogenates were prepared from mice of the indicated genotypes at P30. Total, soluble (*Sol.*), and insoluble (*Insol.*) fractions were subjected to immunoblotting with the indicated antibodies. Data were obtained from three independent experiments. *B*, liver cryosections of *Rpt2*$^{f/f}$;*Atg7*$^{f/f}$;Alb mice were double-immunostained with p62 and ubiquitin antibodies. A portion of each image was magnified and shown in the *inset*. *Arrows* indicate large pleomorphic aggregated structures. Merged images are shown in the *right column* (*red*, p62; *green*, ubiquitin). *Bars*, 20 μm. *C*, electron micrographs of *Rpt2*$^{f/f}$;*Atg7*$^{f/f}$;Alb hepatocytes. *Arrowheads* indicate aggregated structures. *Bar*, 1 μm. *D*, growth curves of mice of the indicated genotypes. Data are means ± S.E. of control ($n = 35$), *Atg7*$^{f/f}$;Alb ($n = 22$), *Rpt2*$^{f/f}$;Alb ($n = 10$), and *Rpt2*$^{f/f}$;*Atg7*$^{f/f}$;Alb ($n = 17$) mice. **, $p < 0.01$; ***, $p < 0.001$. *E*, ratio of liver weight to body weight of mice of the indicated genotype at P30. Data are means ± S.E. of control ($n = 19$), *Atg7*$^{f/f}$;Alb ($n = 13$), *Rpt2*$^{f/f}$;Alb ($n = 10$), and *Rpt2*$^{f/f}$;*Atg7*$^{f/f}$;Alb ($n = 8$) mice. *, $p < 0.05$; ***, $p < 0.001$. *F*, H&E staining of livers of the indicated genotypes at P30. *P*, portal triad; *CV*, central vein. *Bar*, 100 μm. *G*, serum levels of aspartate aminotransferase (*AST*), alanine aminotransferase (*ALT*), and alkaline phosphatase (*ALP*) were measured. Data are means ± S.E. of control ($n = 17$), *Atg7*$^{f/f}$;Alb ($n = 13$), *Rpt2*$^{f/f}$;Alb ($n = 8$), and *Rpt2*$^{f/f}$;*Atg7*$^{f/f}$;Alb ($n = 16$) mice. **, $p < 0.01$; ***, $p < 0.001$. *IU/L*, international units/liter.

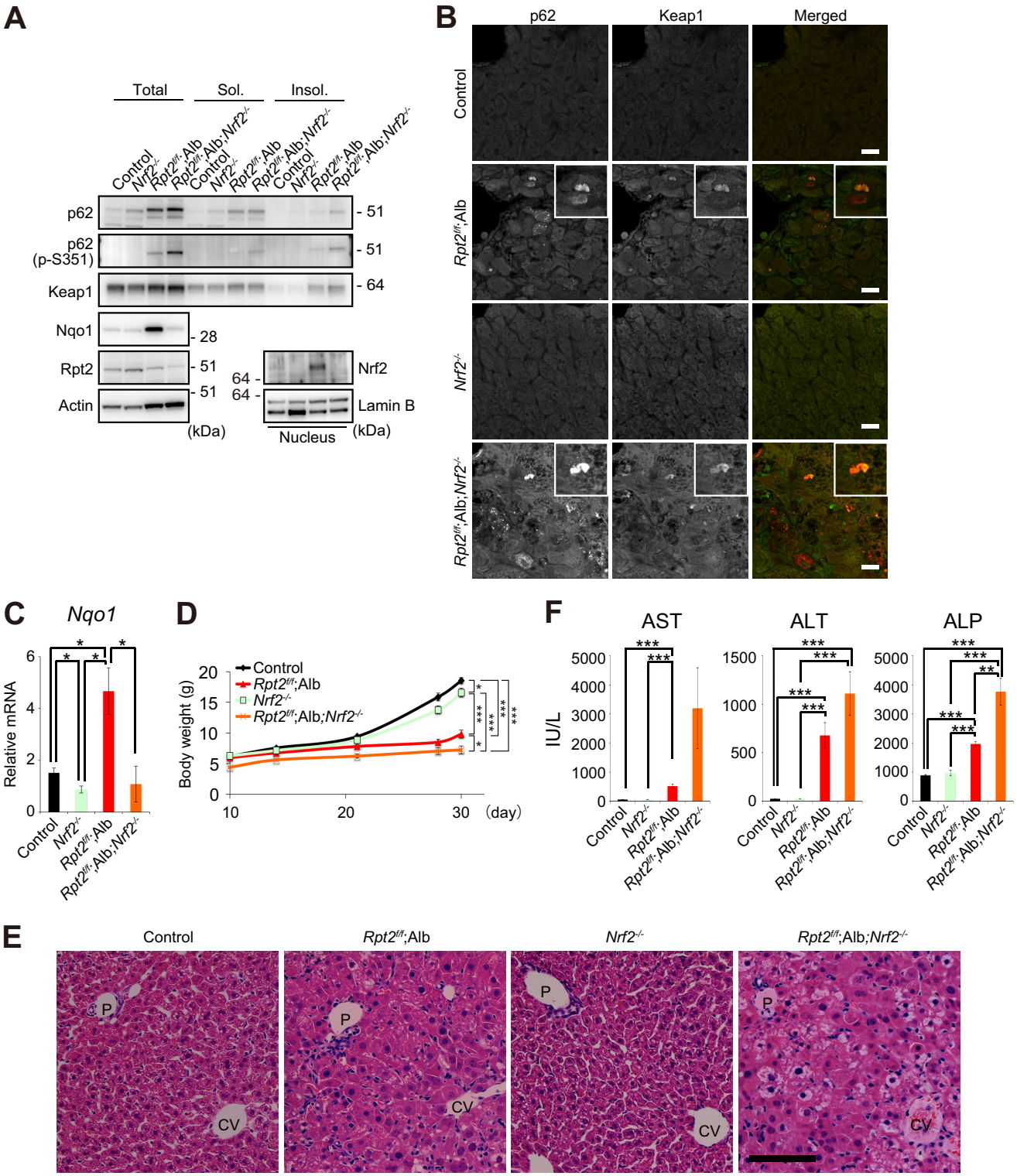

FIGURE 5. **Feedback activation of the Keap1-Nrf2 pathway serves as a physiological adaptation to impaired proteasome function.** *A*, total lysates, detergent-soluble (*Sol.*) and -insoluble (*Insol.*) fractions, and nuclear fractions from livers of the indicated genotypes were subjected to immunoblotting with the indicated antibodies. Data were obtained from three independent experiments. *B*, liver cryosections from mice of the indicated genotypes were double-immunostained with antibodies against p62 and Keap1 antibodies. *Arrows* indicate large pleomorphic aggregated structures. Merged images are shown in the *right column* of each panel (*red*, p62; *green*, Keap1). *Bars*, 20 μm. *C*, total RNAs were prepared from livers of the indicated genotypes. Values were normalized to the amount of mRNA in the livers of control mice. Data are means ± S.E. of control ($n = 14$), *Nrf2*$^{-/-}$ ($n = 10$), *Rpt2*$^{f/f}$;Alb ($n = 5$), and *Rpt2*$^{f/f}$;Alb;*Nrf2*$^{-/-}$ ($n = 7$) mice. *, $p < 0.05$. *D*, growth curves of mice of the indicated genotypes. Data are means ± S.E. of control ($n = 15$), *Nrf2*$^{-/-}$ ($n = 13$), *Rpt2*$^{f/f}$;Alb ($n = 6$), and *Rpt2*$^{f/f}$;Alb;*Nrf2*$^{-/-}$ ($n = 6$) mice. *, $p < 0.05$; ***, $p < 0.001$. *E*, H&E staining of livers of the indicated genotypes at P30. *P*, portal triad; *CV*, central vein. *Bar*, 100 μm. *F*, serum levels of aspartate aminotransferase (*AST*), alanine aminotransferase (*ALT*), and alkaline phosphatase (*ALP*) were measured. Data are means ± S.E. of control ($n = 13$), *Nrf2*$^{-/-}$ ($n = 11$), *Rpt2*$^{f/f}$;Alb ($n = 6$), and *Rpt2*$^{f/f}$;Alb;*Nrf2*$^{-/-}$ ($n = 7$) mice. **, $p < 0.01$; ***, $p < 0.001$. *IU/L*, international units/liter.

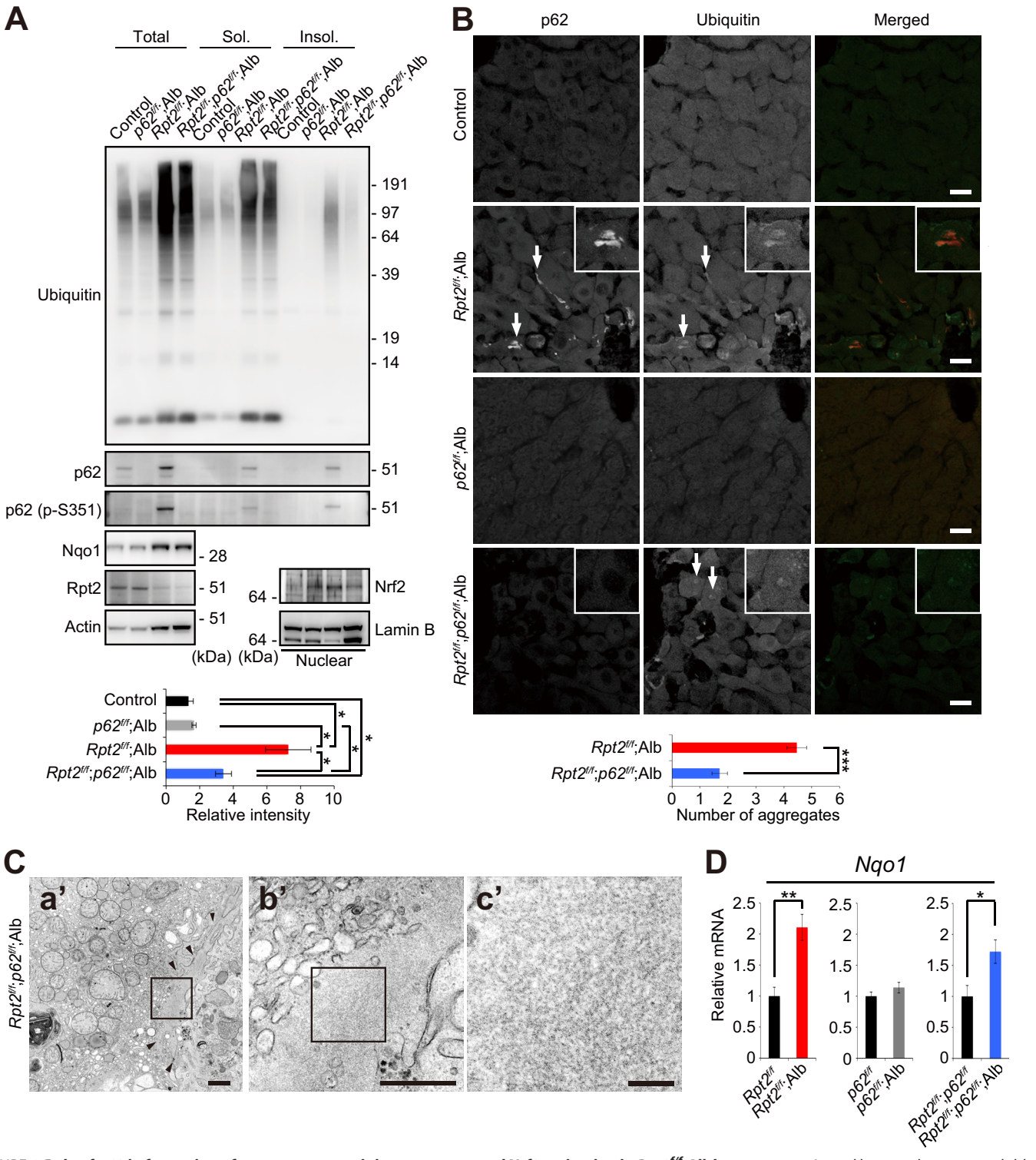

FIGURE 6. **Role of p62 in formation of aggregate-containing structures and Nrf2 activation in *Rpt2$^{f/f}$;Alb* hepatocytes.** *A*, total lysates, detergent-soluble (*Sol.*) and -insoluble (*Insol.*) fractions, and nuclear fractions from livers of the indicated genotypes were subjected to immunoblotting with the indicated antibodies. Data were obtained from three independent experiments. *B*, liver cryosections from mice of the indicated genotypes were double-immunostained with p62 and ubiquitin antibodies. A portion of each image is magnified and shown in the *inset*. *Arrows* indicate large pleomorphic aggregated structures. Merged images are shown in the *right column* (*red*, p62; *green*, ubiquitin). *Bars*, 20 μm. The graph shows the average number (± S.E.) of ubiquitin-positive large aggregates counted in an area of 210 × 210 μm in liver sections from three animals for each genotype ($n = 30$). *C*, electron micrograph of *Rpt2$^{f/f}$;p62$^{f/f}$;*Alb hepatocytes. The *boxed* regions in *a'* and *b'* are *enlarged* and shown in *b'* and *c'*, respectively. *Arrowheads* indicate aggregated structures. *Bars*, *a'*, 1 μm; *b'*, 0.5 μm; *c'*, 0.1 μm. *D*, total RNAs were prepared from livers of the indicated genotypes. Values were normalized to the amount of mRNA in the livers of control mice. Data are means ± S.E. of *Rpt2$^{f/f}$* ($n = 4$), *Rpt2$^{f/f}$;*Alb ($n = 8$), *p62$^{f/f}$* ($n = 13$), *p62$^{f/f}$;*Alb ($n = 10$), *Rpt2$^{f/f}$;p62$^{f/f}$* ($n = 11$), and *Rpt2$^{f/f}$;p62$^{f/f}$;*Alb ($n = 12$) mice. *, $p < 0.05$; **, $p < 0.01$.

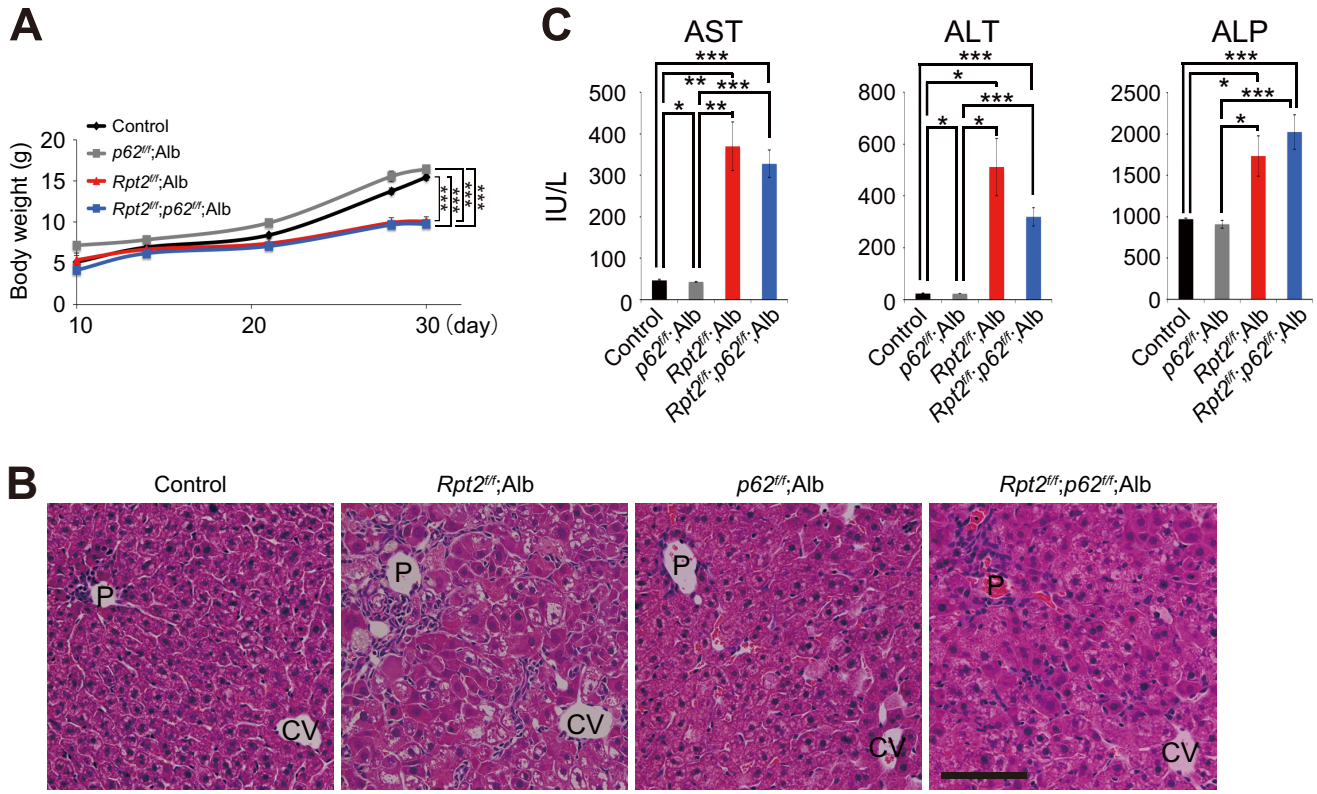

FIGURE 7. **Pathology in *Rpt2$^{f/f}$;Alb* liver by concomitant loss of p62.** *A*, growth curves of mice of the indicated genotypes. Data are means ± S.E. of control ($n = 44$), *p62$^{f/f}$*;Alb ($n = 9$), *Rpt2$^{f/f}$*;Alb ($n = 6$), and *Rpt2$^{f/f}$;p62$^{f/f}$*;Alb ($n = 15$) mice. ***, $p < 0.001$. *B*, H&E staining of livers of the indicated genotypes at P30. *P*, portal triad; *CV*, central vein. *Bar*, 100 μm. *C*, serum levels of aspartate aminotransferase (*AST*), alanine aminotransferase (*ALT*), and alkaline phosphatase (*ALP*) were measured. Data are means ± S.E. of control ($n = 31$), *p62$^{f/f}$*;Alb ($n = 5$), *Rpt2$^{f/f}$*;Alb ($n = 5$), and *Rpt2$^{f/f}$;p62$^{f/f}$*;Alb ($n = 12$) mice. *, $p < 0.05$; **, $p < 0.01$; ***, $p < 0.001$.

other words, the effect of phosphorylated p62 on Nrf2 activation might be hidden by the robust activation of Nrf2 that occurs in response to impairment of the ubiquitin-proteasome system. In conclusion, our data show for the first time that both elimination of aggregate structures by autophagy and activation of Nrf2 under proteasome-defective conditions serve as physiological adaptations to impaired proteasome function *in vivo*.

Acknowledgments—We thank Y. Yang (Tokyo Metropolitan Institute of Medical Science) for excellent technical assistance and K. Kanno and A. Yabashi (Fukushima Medical University School of Medicine) for assistance with histological studies.

REFERENCES

1. Goldberg, A. L. (2003) Protein degradation and protection against misfolded or damaged proteins. *Nature* **426,** 895–899
2. Finley, D. (2009) Recognition and processing of ubiquitin-protein conjugates by the proteasome. *Annu. Rev. Biochem.* **78,** 477–513
3. Murata, S., Yashiroda, H., and Tanaka, K. (2009) Molecular mechanisms of proteasome assembly. *Nat. Rev. Mol. Cell Biol.* **10,** 104–115
4. Mizushima, N., and Levine, B. (2010) Autophagy in mammalian development and differentiation. *Nat Cell Biol.* **12,** 823–830
5. Mizushima, N., and Komatsu, M. (2011) Autophagy: renovation of cells and tissues. *Cell* **147,** 728–741
6. Rubinsztein, D. C. (2006) The roles of intracellular protein-degradation pathways in neurodegeneration. *Nature* **443,** 780–786
7. Rubinsztein, D. C., Mariño, G., and Kroemer, G. (2011) Autophagy and aging. *Cell* **146,** 682–695
8. Kirkin, V., McEwan, D. G., Novak, I., and Dikic, I. (2009) A role for ubiquitin in selective autophagy. *Mol. Cell* **34,** 259–269
9. Youle, R. J., and Narendra, D. P. (2011) Mechanisms of mitophagy. *Nat. Rev. Mol. Cell Biol.* **12,** 9–14
10. Deretic, V., and Levine, B. (2009) Autophagy, immunity, and microbial adaptations. *Cell Host Microbe* **5,** 527–549
11. Pandey, U. B., Nie, Z., Batlevi, Y., McCray, B. A., Ritson, G. P., Nedelsky, N. B., Schwartz, S. L., DiProspero, N. A., Knight, M. A., Schuldiner, O., Padmanabhan, R., Hild, M., Berry, D. L., Garza, D., Hubbert, C. C., Yao, T. P., Baehrecke, E. H., and Taylor, J. P. (2007) HDAC6 rescues neurodegeneration and provides an essential link between autophagy and the UPS. *Nature* **447,** 859–863
12. Iwata, A., Christianson, J. C., Bucci, M., Ellerby, L. M., Nukina, N., Forno, L. S., and Kopito, R. R. (2005) Increased susceptibility of cytoplasmic over nuclear polyglutamine aggregates to autophagic degradation. *Proc. Natl. Acad. Sci. U.S.A.* **102,** 13135–13140
13. Iwata, A., Riley, B. E., Johnston, J. A., and Kopito, R. R. (2005) HDAC6 and microtubules are required for autophagic degradation of aggregated huntingtin. *J. Biol. Chem.* **280,** 40282–40292
14. Narendra, D., Tanaka, A., Suen, D. F., and Youle, R. J. (2008) Parkin is recruited selectively to impaired mitochondria and promotes their autophagy. *J. Cell Biol.* **183,** 795–803
15. Narendra, D. P., Jin, S. M., Tanaka, A., Suen, D. F., Gautier, C. A., Shen, J., Cookson, M. R., and Youle, R. J. (2010) PINK1 is selectively stabilized on impaired mitochondria to activate Parkin. *PLoS Biol.* **8,** e1000298
16. Manzanillo, P. S., Ayres, J. S., Watson, R. O., Collins, A. C., Souza, G., Rae, C. S., Schneider, D. S., Nakamura, K., Shiloh, M. U., and Cox, J. S. (2013) The ubiquitin ligase parkin mediates resistance to intracellular pathogens. *Nature* **501,** 512–516
17. Huett, A., Heath, R. J., Begun, J., Sassi, S. O., Baxt, L. A., Vyas, J. M., Goldberg, M. B., and Xavier, R. J. (2012) The LRR and RING domain protein LRSAM1 is an E3 ligase crucial for ubiquitin-dependent autophagy of intracellular *Salmonella typhimurium*. *Cell Host Microbe* **12,**

778–790
18. Bjørkøy, G., Lamark, T., Brech, A., Outzen, H., Perander, M., Overvatn, A., Stenmark, H., and Johansen, T. (2005) p62/SQSTM1 forms protein aggregates degraded by autophagy and has a protective effect on huntingtin-induced cell death. *J. Cell Biol.* **171,** 603–614
19. Kirkin, V., Lamark, T., Sou, Y. S., Bjørkøy, G., Nunn, J. L., Bruun, J. A., Shvets, E., McEwan, D. G., Clausen, T. H., Wild, P., Bilusic, I., Theurillat, J. P., Øvervatn, A., Ishii, T., Elazar, Z., Komatsu, M., Dikic, I., and Johansen, T. (2009) A role for NBR1 in autophagosomal degradation of ubiquitinated substrates. *Mol. Cell* **33,** 505–516
20. Thurston, T. L., Ryzhakov, G., Bloor, S., von Muhlinen, N., and Randow, F. (2009) The TBK1 adaptor and autophagy receptor NDP52 restricts the proliferation of ubiquitin-coated bacteria. *Nat. Immunol.* **10,** 1215–1221
21. Wild, P., Farhan, H., McEwan, D. G., Wagner, S., Rogov, V. V., Brady, N. R., Richter, B., Korac, J., Waidmann, O., Choudhary, C., Dötsch, V., Bumann, D., and Dikic, I. (2011) Phosphorylation of the autophagy receptor optineurin restricts Salmonella growth. *Science* **333,** 228–233
22. Zatloukal, K., Stumptner, C., Fuchsbichler, A., Heid, H., Schnoelzer, M., Kenner, L., Kleinert, R., Prinz, M., Aguzzi, A., and Denk, H. (2002) p62 Is a common component of cytoplasmic inclusions in protein aggregation diseases. *Am. J. Pathol.* **160,** 255–263
23. Hayes, J. D., and McMahon, M. (2009) NRF2 and KEAP1 mutations: permanent activation of an adaptive response in cancer. *Trends Biochem. Sci* **34,** 176–188
24. Jaramillo, M. C., and Zhang, D. D. (2013) The emerging role of the Nrf2-Keap1 signaling pathway in cancer. *Genes Dev.* **27,** 2179–2191
25. Komatsu, M., Kurokawa, H., Waguri, S., Taguchi, K., Kobayashi, A., Ichimura, Y., Sou, Y. S., Ueno, I., Sakamoto, A., Tong, K. I., Kim, M., Nishito, Y., Iemura, S., Natsume, T., Ueno, T., Kominami, E., Motohashi, H., Tanaka, K., and Yamamoto, M. (2010) The selective autophagy substrate p62 activates the stress responsive transcription factor Nrf2 through inactivation of Keap1. *Nat. Cell Biol.* **12,** 213–223
26. Ichimura, Y., Waguri, S., Sou, Y. S., Kageyama, S., Hasegawa, J., Ishimura, R., Saito, T., Yang, Y., Kouno, T., Fukutomi, T., Hoshii, T., Hirao, A., Takagi, K., Mizushima, T., Motohashi, H., Lee, M. S., Yoshimori, T., Tanaka, K., Yamamoto, M., and Komatsu, M. (2013) Phosphorylation of p62 activates the Keap1-Nrf2 pathway during selective autophagy. *Mol. Cell* **51,** 618–631
27. Taguchi, K., Fujikawa, N., Komatsu, M., Ishii, T., Unno, M., Akaike, T., Motohashi, H., and Yamamoto, M. (2012) Keap1 degradation by autophagy for the maintenance of redox homeostasis. *Proc. Natl. Acad. Sci. U.S.A.* **109,** 13561–13566
28. Bae, S. H., Sung, S. H., Oh, S. Y., Lim, J. M., Lee, S. K., Park, Y. N., Lee, H. E., Kang, D., and Rhee, S. G. (2013) Sestrins activate Nrf2 by promoting p62-dependent autophagic degradation of Keap1 and prevent oxidative liver damage. *Cell Metab.* **17,** 73–84
29. Matsumoto, G., Wada, K., Okuno, M., Kurosawa, M., and Nukina, N. (2011) Serine 403 phosphorylation of p62/SQSTM1 regulates selective autophagic clearance of ubiquitinated proteins. *Mol. Cell* **44,** 279–289
30. Pilli, M., Arko-Mensah, J., Ponpuak, M., Roberts, E., Master, S., Mandell, M. A., Dupont, N., Ornatowski, W., Jiang, S., Bradfute, S. B., Bruun, J. A., Hansen, T. E., Johansen, T., and Deretic, V. (2012) TBK-1 promotes autophagy-mediated antimicrobial defense by controlling autophagosome maturation. *Immunity* **37,** 223–234
31. Bedford, L., Hay, D., Devoy, A., Paine, S., Powe, D. G., Seth, R., Gray, T., Topham, I., Fone, K., Rezvani, N., Mee, M., Soane, T., Layfield, R., Sheppard, P. W., Ebendal, T., Usoskin, D., Lowe, J., and Mayer, R. J. (2008) Depletion of 26S proteasomes in mouse brain neurons causes neurodegeneration and Lewy-like inclusions resembling human pale bodies. *J. Neurosci.* **28,** 8189–8198
32. Postic, C., Shiota, M., Niswender, K. D., Jetton, T. L., Chen, Y., Moates, J. M., Shelton, K. D., Lindner, J., Cherrington, A. D., and Magnuson, M. A. (1999) Dual roles for glucokinase in glucose homeostasis as determined by liver and pancreatic beta cell-specific gene knock-outs using Cre recombinase. *J. Biol. Chem.* **274,** 305–315
33. Komatsu, M., Waguri, S., Koike, M., Sou, Y. S., Ueno, T., Hara, T., Mizushima, N., Iwata, J., Ezaki, J., Murata, S., Hamazaki, J., Nishito, Y., Iemura, S., Natsume, T., Yanagawa, T., Uwayama, J., Warabi, E., Yoshida, H., Ishii, T., Kobayashi, A., Yamamoto, M., Yue, Z., Uchiyama, Y., Kominami, E., and Tanaka, K. (2007) Homeostatic levels of p62 control cytoplasmic inclusion body formation in autophagy-deficient mice. *Cell* **131,** 1149–1163
34. Harada, H., Warabi, E., Matsuki, T., Yanagawa, T., Okada, K., Uwayama, J., Ikeda, A., Nakaso, K., Kirii, K., Noguchi, N., Bukawa, H., Siow, R. C., Mann, G. E., Shoda, J., Ishii, T., and Sakurai, T. (2013) Deficiency of p62/sequestosome 1 causes hyperphagia due to leptin resistance in the brain. *J. Neurosci.* **33,** 14767–14777
35. Itoh, K., Chiba, T., Takahashi, S., Ishii, T., Igarashi, K., Katoh, Y., Oyake, T., Hayashi, N., Satoh, K., Hatayama, I., Yamamoto, M., and Nabeshima, Y. (1997) An Nrf2/small Maf heterodimer mediates the induction of phase II detoxifying enzyme genes through antioxidant response elements. *Biochem. Biophys. Res. Commun.* **236,** 313–322
36. Tanida, I., Mizushima, N., Kiyooka, M., Ohsumi, M., Ueno, T., Ohsumi, Y., and Kominami, E. (1999) Apg7p/Cvt2p: a novel protein-activating enzyme essential for autophagy. *Mol. Biol. Cell* **10,** 1367–1379
37. Kaneko, T., Hamazaki, J., Iemura, S., Sasaki, K., Furuyama, K., Natsume, T., Tanaka, K., and Murata, S. (2009) Assembly pathway of the Mammalian proteasome base subcomplex is mediated by multiple specific chaperones. *Cell* **137,** 914–925
38. Komatsu, M., Waguri, S., Chiba, T., Murata, S., Iwata, J., Tanida, I., Ueno, T., Koike, M., Uchiyama, Y., Kominami, E., and Tanaka, K. (2006) Loss of autophagy in the central nervous system causes neurodegeneration in mice. *Nature* **441,** 880–884
39. Waguri, S., and Komatsu, M. (2009) Biochemical and morphological detection of inclusion bodies in autophagy-deficient mice. *Methods Enzymol.* **453,** 181–196
40. Wang, E. Y., Yeh, S. H., Tsai, T. F., Huang, H. P., Jeng, Y. M., Lin, W. H., Chen, W. C., Yeh, K. H., Chen, P. J., and Chen, D. S. (2011) Depletion of beta-catenin from mature hepatocytes of mice promotes expansion of hepatic progenitor cells and tumor development. *Proc. Natl. Acad. Sci. U.S.A.* **108,** 18384–18389
41. Kabeya, Y., Mizushima, N., Ueno, T., Yamamoto, A., Kirisako, T., Noda, T., Kominami, E., Ohsumi, Y., and Yoshimori, T. (2000) LC3, a mammalian homologue of yeast Apg8p, is localized in autophagosome membranes after processing. *EMBO J.* **19,** 5720–5728